Two-component density functional theory study of quantized muons in solids

Li Deng,[1,*] Yue Yuan,[1,2,*] Francis L. Pratt,[2] Wenshuai Zhang,[3] Ziwen Pan,[1,†] and Bangjiao Ye[1,‡]

[1]*State Key Laboratory of Particle Detection and Electronics, University of Science and Technology of China, Hefei 230026, China*

[2]*ISIS Facility, STFC Rutherford Appleton Laboratory, Chilton, Oxfordshire OX11 0QX, United Kingdom*

[3]*Supercomputing Center, Network Information Center, University of Science and Technology of China, Hefei 230026, China*

(Received 16 December 2022; revised 1 March 2023; accepted 21 March 2023; published 28 March 2023)

The quantum effect of light nuclei in materials is usually considered as lattice vibration and zero-point motion from an *ab initio* perspective. Here we start from full-quantized particles and take the muon as an example, considering the two-body quantized system of the muon and the electrons within two-component density functional theory, which can calculate the related two-body wave functions directly and automatically taking into account the quantum effect of the muon. We first simulate the two-body correlation energy and the pair-correlation function by quantum Monte Carlo, then construct a two-body self-consistent loop to solve the two-body density and then the hyperfine couplings are estimated. This is an attempt to reveal the quantum effect of light nuclei in materials from a different perspective. We finally find this fundamental method agrees better with experiments and shows good potential for further such calculations.

DOI: 10.1103/PhysRevB.107.094433

I. INTRODUCTION

Quantum zero-point motion (ZPM) of nuclei plays an important role in materials that contain light nuclei (mainly the hydrogen nuclei, but also some other particles like the positive muon, deuterium, tritium, etc.). In the case of implanted positive muon (μ^+, simply abbreviated as muon below) in muon spin relaxation (μ^+SR) technology, a beam of the polarized muon is injected into materials, the local magnetic field of the stopping muon can be inferred from the angular distribution of the decay positrons due to the procession of muon spin under the local magnetic field. The quantum ZPM of the stopping muon would directly influence the experiments due to the light mass of the muon ($\sim 1/9$ of a proton). Since μ^+SR can give a high-accuracy experimental observation of the hyperfine couplings of the muon in materials, it becomes possible to study the quantum effect of the muon in calculations and may be further extended to other such situations such as hydrogen in materials.

In earlier works, as density functional theory (DFT) can effectively predict the local position of the muon in host materials, the contact hyperfine magnetic field or muon spin evolution at muon sites are calculated [1–9]. These works are based on point-like muon and some of them considered the ZPM effect of muon or atoms by vibrational states and improve the agreement with experiment than point-like case [1,7,9,10]. However, on the one hand, the accuracy can also be further improved. On the other hand, most of the present works use the phonon method, which is based on some approximation (harmonic approximation, for example) and is restricted in different species of materials. Thus, a common and accurate method which can naturally include the quantum effect of light nuclei like the muon is worth being improved.

Within the framework of DFT, two-component density functional theory (TCDFT) is an algorithm that naturally contains the quantum effect of both components. This algorithm has been successfully implanted into the positron-electron system [11–14]. Intuitively, muon can also be treated as a heavier positron (while in previous works it is usually treated as a lighter nucleus), which plays a similar role with electrons in materials, thus the quantum effect of the muon is completely included without further dealing. The key problem of TCDFT, as well as the normal DFT for electronic systems, is the exchange-correlation functional, which cannot be expressed by a simple analytical formula and is usually parametrized by a further approach (taking the density as the only variable). Local density approximation (LDA) is the simplest and roughest one. By assuming that all interaction energy terms are only dependent on the density of the electrons (and the density of the other component in TCDFT), the exchange-correlation functional can be parametrized through some accurate energy calculations in homogenous gas systems. This should be the first step in muon-electron DFT study. Another reason for limiting more degrees of freedom such as the gradient of density is that the correlation functional of the muon-electron already has two variables (the density of the muon and electron) because of the localized states of the muon. Thus, in this work, we simulate a series of homogenous muon-electron gas systems and parametrize the correlation energy form of $E_c(n^+, n^-)$ within LDA, then it is possible to calculate the density of the muon directly using TCDFT.

Another problem arises from the calculation of the hyperfine couplings. If the muon is treated as a fixed point with the Born-Oppenheimer (BO) approximation, some methods are able to calculate the contact (spin) density of the

*These authors contributed equally to this work.

†panzw19@ustc.edu.cn

‡bjye@ustc.edu.cn

electrons (projector augmented-wave and its reconstruction method [15], for example), thus the hyperfine couplings of the muon can be estimated. However, when the quantum effect of the muon is expected to be included, it is no longer suitable to treat the muon as a point. Although some previous works considered the ZPM and the wave function of the muon by other approaches, the muon is usually treated as the points sampling by its wave function, where the BO approximation still plays a role. Using a pair-correlation function (PCF) together with TCDFT we are able to estimate the true contact two-body density from the calculated one-body density, so it is also introduced in this work.

In other words, what we are considering here differs from the nucleus-like muon and the phonon methods in several respects.

(1) Both the muon and the electrons are fully quantized. The wave functions of the electrons and the muon are calculated from the Kohn-Sham equation and single-particle Schrödinger equation, respectively, each being self-consistent with the other. The vibrational states of the muon and some relative approaches are unnecessary.

(2) The interaction between the muon and the electrons is described by the Coulomb potential and correlation potential of their density.

(3) The contact density enhancement is described by the PCF.

The correlation energy and the PCF are simulated using the variational Monte Carlo (VMC) and diffusion Monte Carlo (DMC) methods [16,17] as implemented in CASINO [18], then parametrized by LDA. Thus the contact spin density can be calculated directly from the two-body wave function and the BO approximation of the muon is completely abandoned.

II. TCDFT SYSTEM

TCDFT is a DFT-based theory to study two-body systems, the most widely used example of TCDFT may be the positron-annihilation lifetime calculation. When the switch is made from the positron-electrons system to the muon-electrons system, the fundamental equations (without spin) are

$$\left[-\tfrac{1}{2}\nabla^2 + V_{\text{ion}}^- + V_H + V_{\text{xc}} + V_{\text{coul}}^- + V_{\text{corr}}^-\right]\psi^- = \varepsilon^-\psi^- \quad (1)$$

for the electrons (Kohn-Sham equation) and

$$\left[-\frac{1}{2M}\nabla^2 + V_{\text{ion}}^+ + V_{\text{coul}}^+ + V_{\text{corr}}^+\right]\psi^+ = \varepsilon^+\psi^+ \quad (2)$$

for the muon (single-particle Schrödinger equation). Where V_{ion} is the Coulomb potential from the positive nuclei in the material or the pseudopotential from the ions. V_H is the Hartree potential of electrons (or of the valence electrons in the case of the pseudopotential). V_{xc} is the exchange-correlation potential between electrons. V_{coul} is the Coulomb potential from the muon to electrons or from electrons to the muon. V_{corr} is the two-body correlation potential and ψ is the wave function. M is the mass of the muon. There is only one muon present in the sample at any time, so there is no muon-muon interaction term.

The two-body correlation potential can be expressed as

$$V_{\text{corr}}^{\pm} = \frac{\delta E_{\text{corr}}[n_+, n_-]}{\delta n_{\pm}}, \quad (3)$$

where E_{corr} is the two-body correlation energy, which can be estimated from the relaxation energy of the homogeneous system in QMC. It is worth noting that the correlation energy functional is not unique, different approximations may give completely different results. Different approximation here means not only the chosen parametric form (LDA, GGA, or something else), but also the simulation method of the standard systems (the QMC of homogenous systems, ZPE of vibrational states of some molecular systems [19], for example). In this work, a simple form simulated by QMC and parametrized within LDA is used, as discussed below.

The next step is to apply the local spin density approximation (LSDA) method to Eqs. (1) and (2). The equations become

$$\left[-\tfrac{1}{2}\nabla^2 + V_{\text{ion}}^- + V_H + V_{\text{xc}} + V^- + V_{\text{corr}}^- - \mu_B B_{\text{xc}}\right]\psi_\uparrow^- = \varepsilon_\uparrow^-\psi^-, \quad (4)$$

$$\left[-\tfrac{1}{2}\nabla^2 + V_{\text{ion}}^- + V_H + V_{\text{xc}} + V_{\text{coul}}^- + V_{\text{corr}}^- + \mu_B B_{\text{xc}}\right]\psi_\downarrow^- = \varepsilon_\downarrow^-\psi^-, \quad (5)$$

where $\uparrow$ and $\downarrow$ stand for spin-up and spin-down electrons, respectively, and B_{xc} is the so-called local exchange-correlation magnetic field of electrons. Because the magnetic moment of the muon is much smaller than that of the electron, assuming that the spin state of the muon does not influence the electrons' states. Considering that the spin states of the muon are thought to be detected by experiments and are not calculated here, thus Eq. (2) does not divide into two parts.

Within the framework of TCDFT, the calculated wave function is the one-body wave function from the average field, the product of the one-body density of electrons and the muon is not the true two-body density. The enhancement contact effect can be described by PCF:

$$\gamma_{\alpha\beta}(\mathbf{r}, \mathbf{r}') = N_\alpha(N_\beta - \delta_{\alpha\beta}) \cdot \frac{\int \Psi^*(\mathbf{r}, \mathbf{r}', \mathbf{r_3}, \ldots, \mathbf{r_N})\Psi(\mathbf{r}, \mathbf{r}', \mathbf{r_3}, \ldots, \mathbf{r_N})d\mathbf{r_3}\ldots d\mathbf{r_N}}{\int \Psi^*(\mathbf{r_1}, \mathbf{r_2}, \ldots, \mathbf{r_N})\Psi(\mathbf{r_1}, \mathbf{r_2}, \ldots, \mathbf{r_N})d\mathbf{R}}, \quad (6)$$

or

$$\gamma_{\alpha\beta}(\mathbf{r}, \mathbf{r}') = n_\alpha(\mathbf{r})n_\beta(\mathbf{r}')g_{\alpha\beta}(\mathbf{r}, \mathbf{r}'), \quad (7)$$

where γ signifies the diagonal elements of the two-particle density matrix. α, β are particle symbols, with mass, charge, and spin($\uparrow$ or $\downarrow$). Here α and β stand for muon(s) and electron(s), respectively (γ is thought to be independent of the spin due to LDA). $\mathbf{r}$ is the particle coordinate, Ψ is the many-body wave function, N is the total number of particles, n is the one-body density of particles. g is the PCF, which stands for the enhancement from one-body density to true two-body density. What we are interested in here is the zero distance enhancement, which means the contact density enhancement of the muon and electrons, $g_{\mu,e}(\mathbf{r_e} = \mathbf{r}_\mu, n^+, n^-)$, written as $g(0; n^+, n^-)$ or $g(0)$.

In summary, the equations we actually solve are Eqs. (4), (5), and (2) . The hyperfine contact field of the muon is obtained from

$$B_{\text{cont}} = \int \frac{2\mu_0}{3}\mu_B \rho_s(\mathbf{r}) g(0;\mathbf{r})|\psi_\mu(\mathbf{r})|^2 d^3\mathbf{r}, \tag{8}$$

where B_{cont} is the contact hyperfine field, μ_0 is the permeability of the vacuum, μ_B is the magnetic moment of the electron, ρ_s is the spin density of electrons obtained from TCDFT, and $\mathbf{r}$ is the spatial coordinate of the muon, $g(0;\mathbf{r})$ is the $g[0; n^+(\mathbf{r}), n^-(\mathbf{r})]$. Additionally we can use the the contact hyperfine coupling A:

$$A = \int \frac{2\mu_0}{3}\gamma_e\gamma_\mu \rho_s(\mathbf{r}_\mu) g(0;\mathbf{r})|\psi_\mu(\mathbf{r})|^2 d^3\mathbf{r}. \tag{9}$$

γ_e is the electron gyromagnetic ratio and γ_μ is the muon gyromagnetic ratio.

III. QMC STUDY OF THE PCF AND CORRELATION ENERGY

Now some QMC simulation is necessary for the parametric form of the PCF and the two-body correlation energy. A similar QMC simulation has been done in the positron-electron system [20]. Within the LDA, the PCF and the correlation energy are described by a functional of the density component of the electrons and the muon, thus homogeneous gas systems for the muon and the electrons are simulated.

A Slater-Jastrow-backflow (SJB) [21,22] trial wave function is used with plane-wave orbits

$$\Psi_{\text{PW}}^{\text{SJB}} = e^{J(\mathbf{R})}[\phi_i(\mathbf{r}_\uparrow^- + \xi(\mathbf{R}))][\phi_j(\mathbf{r}_\downarrow^- + \xi(\mathbf{R}))] \cdot [\phi_I(\mathbf{r}_\uparrow^+ + \xi(\mathbf{R}))][\phi_J[\mathbf{r}_\downarrow^+ + \xi(\mathbf{R}))], \tag{10}$$

where $\mathbf{R}$ are the positions of all the particles, ϕ is the plane-wave basis. $\mathbf{r}_\uparrow^-$ and $\mathbf{r}_\downarrow^-$ are the positions of up- and down-spin electrons, respectively (a similar definition for $\mathbf{r}^+$), and [...] denotes a Slater determinant. $J(\mathbf{R})$ is the Jastrow exponent and $\xi(\mathbf{R})$ is the backflow displacement.

The Jastrow exponents are first optimized using the VMC variance-minimum scheme [23]. Then all parameters are optimized together and then a DMC calculation is done.

In the main results of this work, only the u term is used in the Jastrow exponent. The DMC time step is set to 0.001 a.u. The spin dependence is set to be 1 ($u_{\mu,\mu} \neq u_{\mu,e} \neq u_{e,e}$). The PCF and correlation energy results are directly estimated from DMC calculation. The target population of walkers of DMC is 1000. There may be some possible ways to improve the accuracy of QMC.

(1) Use several different time steps of DMC in each system and extrapolate the energy linearly to zero time step and/or use the average of the PCF.

(2) Include more correlation terms, the p term of the Jastrow exponent, for example. Or set more particle groups for the u term (increase the spin dep. parameter).

Although the QMC calculations are not as accurate as possible in this work due to the large number of systems to be calculated, the results can still be used as an approximation (an example of the finite-size error is shown in Table I, the p term becomes important for achieving consistent results in large systems). It should be noticed that, because the correlation energy can be sensitive to tge $1e-4$ a.u. level of the total energy per particle, more accurate QMC simulations are worth being improved upon (the PCFs do not change obviously when improving the wave function or expanding the simulation cell size). Some calculated $g(r)$ are shown in Fig. 1 as examples.

TABLE I. The calculation stability of $n^+ \gg n^-$, $r_s^+ = 0.3$. E_{VMC} and E_{DMC} are in a.u. per particle, while var. of VMC and V_{corr}^- are in a.u. The V_{corr}^- is gotten from the total energy difference between the system with and without electron(s), and divided by N_e. In this work, half of the particles are spin-up and the other half are spin-down.

N_μ	N_e	If [a]	E_{VMC}	Var. of VMC	E_{DMC}	V_{corr}^-
28	0	F	−2.4528	0.6248	−2.4713	
28	1	F	−2.3995	1.2502	−2.4214	−1.0251
28	0	T	−2.4579	0.3576	−2.4714	
28	1	T	−2.3996	0.7574	−2.4205	−0.9941
54	0	F	−2.4479	0.9225	−2.4676	
54	1	F	−2.4197	1.3373	−2.4398	−0.9371
54[b]	2	F	−2.3935	1.8710	−2.4133	−0.9476
54	0	T	−2.4533	0.5786	−2.4673	
54	1	T	−2.4186	1.0958	−2.4395	−0.9410
54	2	T	−2.3944	1.4516	−2.4133	−0.9571
108	0	F	−2.4444	1.5329	−2.4603	
108	1	F	−2.4274	2.0411	−2.4436	−0.6410
108	2	F	−2.4120	2.3260	−2.4293	−0.7572
108	0	T	−2.4470	1.1700	−2.4602	
108	1	T	−2.4264	1.7628	−2.4437	−0.8833
108	2	T	−2.4133	2.0173	−2.4305	−0.9369

[a]With the p term in Jastrow for both the muon-and-electron and only-muon system, and the use of the particle group of $u_{\mu_\uparrow,\mu_\uparrow} \neq u_{\mu_\uparrow,\mu_\downarrow} \neq u_{\mu,e} \neq u_{e_\uparrow,e_\uparrow} \neq u_{e_\uparrow,e_\downarrow}$ for the muon-and-electron system (while $u_{\uparrow,\uparrow} \neq u_{\uparrow,\downarrow}$ is always used for the only-muon and only-electron system of this work).
[b]Main result setting.

A series of systems with different densities are simulated and a linear interpolation form of $g(0; R, n^-)$ ($R = n^+/n^-$) while $n^+ \sim n^-$ ($0.2 \leqslant R \leqslant 10$) is used, written as g_1, the data points are shown in Tables II and III. When $n^+ \gg n^-$ or $n^+ \ll n^-$, the PCF is fitted by a simple polynomial. [$r_s^+ = (3/4\pi n^+)^{1/3}$, r_s^- also. All units are in a.u. in this article if not declare.] (g_3 is plotted in Fig. 2, g_2 is plotted in Fig. 3)

$$g_2 = g(0, r_s) = 1 + 0.84829 r_s + 1.2337 r_s^2 - 0.33670 r_s^3 + 0.10023 r_s^4, (n^+ \gg n^-, r_s = r_s^+), \tag{11}$$

$$g_3 = g(0, r_s) = 1 + 2.0047 r_s + 0.16537 r_s^2 - 0.83218 r_s^3 + 0.06222 r_s^4, (n^+ \ll n^-, r_s = r_s^-). \tag{12}$$

Note that g_2 and g_3 here do not satisfy the low-density limit (where g should be expanded to r_s^3 with a specific three-order coefficient) because, in our calculation, this density region does not exist and thus a simple form with high goodness is used.

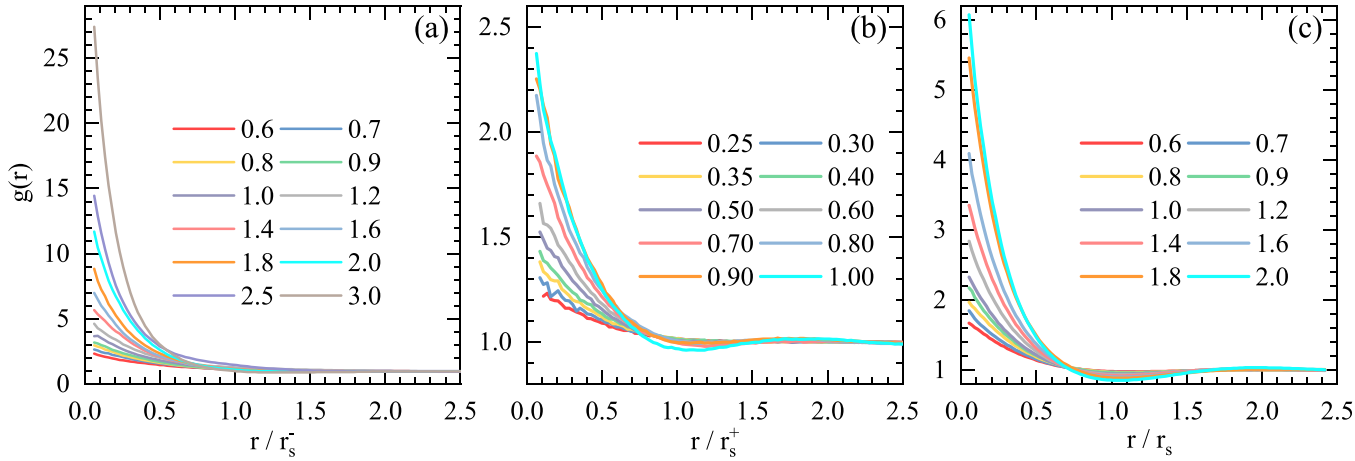

FIG. 1. Some $g(r)$ results. $r_s^- = (3/4\pi n^-)^{1/3}$, r_s^+ also. (a) PCF calculated from 54 electrons and 2 muons, as a function of distance r and r_s^-, (b) PCF calculated from 54 muons and 2 electrons, as a function of distance r and r_s^+, (c)PCF calculated from 28 muons and 28 electrons, as a function of distance r and muon or electrons density. All $g(0)$ are estimated from the extrapolation of $g(r)$.

The final PCF used in calculation is

$$g(0) = \begin{cases} g_1, & 10 \geqslant R \geqslant 0.2, \\ g_2, & R > 10, \\ g_3, & R < 0.2. \end{cases} \tag{13}$$

As for the two-body correlation energy, it is simulated by

$$E_{c,v} = E_v(N_e + N_\mu) - E_v(N_e) - E_v(N_\mu), \tag{14}$$

where $E_{c,v}$ is the correlation energy per volume, the energy E_v stands for the total energy per volume of the system of the muon-and-electron, only-muon, and only-electron, respectively. Note that this equation is for $n^+ \sim n^-$, if one component is much larger than the other one, the energy of the minor component is not reduced due to the zero-density approximation. The two-body correlation energy per volume for $n^+ \sim n^-$ is well fitted by a similar form with Ref. [19] (data points are also shown in Tables II and III)

$$E_{c,v}(n^+, n^-) = \frac{an^+n^- + bn^-(n^+)^{3/2}}{1 + cn^+n^- + dn^-(n^+)^{3/2}}, \tag{15}$$

where $a = -1.4265e-01$, $b = 1.8365e-02$, $c = 5.2581e-01$, $d = -8.6401e-02$.

In most of the areas where the muon distributes, the condition of $n^+ \gg n^-$ is satisfied (there is ~98% of the muon for $n^+ > 3n^-$). The two-body correlation potential of the muon is ignored because QMC shows a tiny correlation potential (~0.01 a.u.) for $n^\pm$ if $n^\pm \gg n^\mp$, and $V_{\rm corr}^+ = \partial E_{c,v}(n^+, n^-)/\partial n^+$ is also approaching to zero while $n^+ \sim n^-$. Thus only $V_{\rm corr}^-$ is necessary, $V_{\rm corr}^- = \partial E_{c,v}(n^+, n^-)/\partial n^-$ is implanted for $n^+ \sim n^-$, written as V_1. The $V_{\rm corr}^-$ in the condition of $n^+ \gg n^-$ is fitted by (Fig. 4)

$$V_2 = V_{\rm corr}^-(r_s) = \frac{A_{-1}r_s^{-1} + A_0 + A_1 r_s - 0.603 \cdot A_2 r_s^2}{1 + B_1 r_s + A_2 r_s^2}, \tag{16}$$

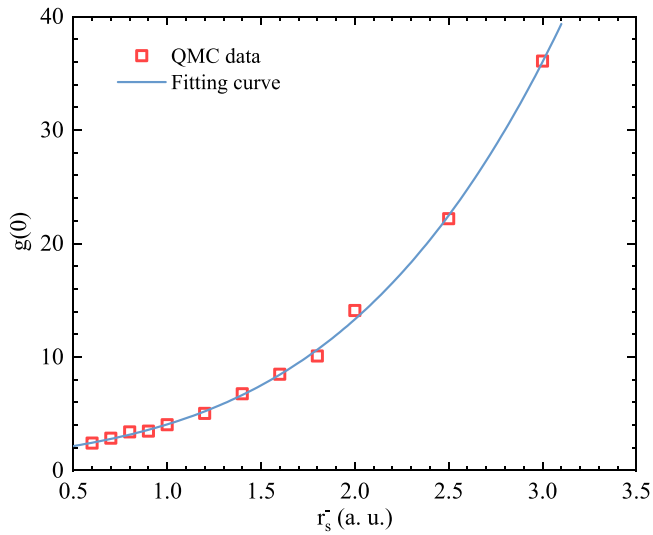

FIG. 2. $g(0)$ for $n^+ \ll n^-$, calculated from 54 electrons and 2 muons system. The fitting curve is the g_3 in Eq. (12).

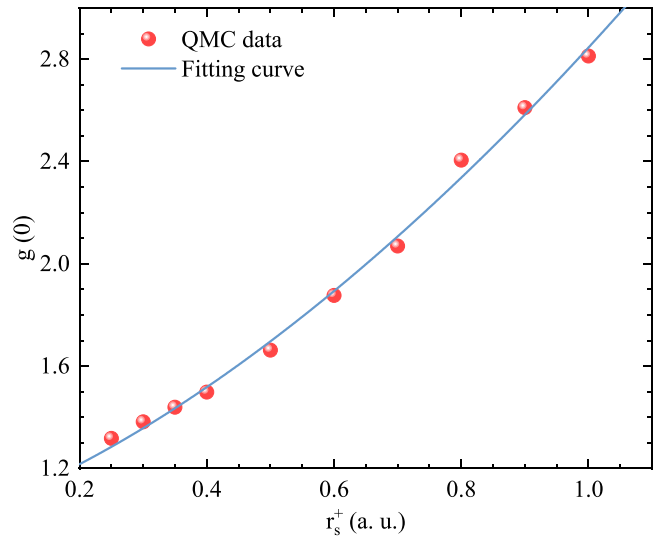

FIG. 3. $g(0)$ for $n^+ \gg n^-$, calculated from 54 muons and 2 electrons system. This corresponds to g_2 in Eq. (11).

TABLE II. $g(0)$ and energy results for $n^+ \sim n^-$ (all units are in a.u.). N_e and N_μ are the number of electrons and muons, respectively. E_{VMC} and E_{DMC} are the total energy per particle of VMC and DMC calculations, respectively. $E_{c,v}$ is the correlation energy per volume. Note that the p term of the Jastrow exponent is not included in these results. These $g(0)$ results are used for the linear interpolation of g_1.

r_s^-	N_e	N_μ	E_{VMC}	Var. of VMC	E_{DMC}	$g(0)$	$E_{c,v}$
0.5	50	10	2.5361	5.5739	2.5301	1.912	−0.079867
0.5	50	20	1.9651	7.9296	1.9573	1.802	−0.11822
0.5	50	30	1.5119	9.2961	1.5026	1.735	−0.14036
0.5	50	40	1.1399	10.506	1.1300	1.668	−0.15361
0.5	50	50	0.82982	11.969	0.81878	1.642	−0.16486
0.5	20	40	0.0045016	9.1490	−0.011308	1.496	−0.21625
0.5	20	60	−0.65883	11.498	−0.67614	1.426	−0.23487
0.5	10	40	−1.0673	7.5686	−1.0868	1.408	−0.25297
0.5	10	50	−1.4161	8.4173	−1.4378	1.370	−0.28931
0.5	6	60	−2.3644	8.1920	−2.3883	1.304	−0.35307
1	50	10	0.34015	1.5389	0.33521	3.608	−0.010138
1	50	20	0.17680	1.9837	0.17026	3.238	−0.015040
1	50	30	0.042346	2.8402	0.035306	3.146	−0.017932
1	50	40	−0.068311	2.6988	−0.075506	2.850	−0.018953
1	50	50	−0.16535	2.9664	−0.17198	2.699	−0.019797
1	20	40	−0.45670	2.0564	−0.46655	2.196	−0.022893
1	20	60	−0.69485	2.2835	−0.70340	2.036	−0.025059
1	10	40	−0.85500	1.5069	−0.86678	1.875	−0.025929
1	10	50	−0.99327	1.7741	−1.0055	1.796	−0.0296620
1	6	60	−1.41380	1.5289	−1.4285	1.602	−0.0335080
1.5	50	10	0.0047909	0.87636	0.0010200	7.349	−0.0032764
1.5	50	20	−0.079582	1.3435	−0.085975	6.586	−0.0049671
1.5	50	30	−0.14743	1.6273	−0.15473	5.945	−0.0058625
1.5	50	40	−0.20428	1.9735	−0.21127	5.132	−0.0061346
1.5	50	50	−0.25261	1.7194	−0.25948	4.351	−0.0061731
1.5	20	40	−0.41731	1.0196	−0.42394	3.301	−0.0065547
1.5	20	60	−0.55155	1.3125	−0.55891	2.789	−0.0068703
1.5	10	40	−0.65030	0.72408	−0.65854	2.434	−0.0074654
1.5	10	50	−0.73377	0.76206	−0.74209	2.374	−0.0077752
1.5	6	60	−1.0034	0.65561	−1.0141	1.934	−0.0086923
2	50	10	−0.087144	0.48578	−0.0914171	13.44	−0.0014769
2	50	20	−0.14516	0.88460	−0.152671	13.11	−0.0023820
2	50	30	−0.18335	1.0327	−0.194159	9.463	−0.0027470
2	50	40	−0.22402	1.4379	−0.231775	9.365	−0.0029621
2	50	50	−0.25209	1.1464	−0.259798	7.120	−0.0028700
2	20	40	−0.36140	0.64263	−0.367448	4.903	−0.0028777
2	20	60	−0.45348	0.66237	−0.458628	3.934	−0.0029746
2	10	40	−0.52126	0.40610	−0.527668	3.572	−0.0029051
2	10	50	−0.58099	0.41474	−0.586912	3.100	−0.0031573
2	8	80	−0.78067	0.45659	−0.787404	2.644	−0.003359

where $A_{-1} = -2.4200\text{e}-1$, $A_0 = -3.7089\text{e}-2$, $A_1 = 3.25863\text{e}-3$, $A_2 = 1.0985\text{e}-2$, $B_1 = -2.6441\text{e}-1$. Here r_s stands for r_s^+. The final correlation potential of the electrons is

$$V_{\text{corr}}^-(n^+, n^-) = \begin{cases} V_1, & R \leqslant 10, \\ V_2 + (V_1 - V_2)e^{-\alpha\cdot(R-10)}, & R > 10. \end{cases} \quad (17)$$

The positive number α would influence the results in some sense. It is necessary due to the lack of high-R correlation potential data. In this work, α is chosen to be 1, to accord with the experimental data of the vacuum case, as shown in Sec. V. Then the parametric form of the PCF and the two-body correlation potential is determined and the contact field can be calculated after Eqs. (4), (5), and (2) are solved.

IV. CALCULATION DETAILS OF TCDFT

To solve Eqs. (4), (5), and (2) with known $V_{\text{corr}}^{\pm}$, a two-body self-consistent loop is introduced, as shown in Fig. 5.

The electronic part of the calculation is carried out using QUANTUM ESPRESSO [24] (QE). V_{ext} is the extra potential produced by the muon. It is introduced as

$$V_{\text{ext}}(\mathbf{r}') = \int \frac{n^+(\mathbf{r})\mathrm{d}^3\mathbf{r}}{|\mathbf{r} - \mathbf{r}'|} + V_{\text{corr}}^-(\mathbf{r}') \quad (18)$$

$$V_{\text{tot}} = V_0 + V_{\text{ext}}, \quad (19)$$

where V_0 is the total potential of the normal QE calculation and V_{tot} is the total potential used in our calculation.

The ground-state wave function of the muon can be solved by the finite difference (FD) method [25] in real space, with

TABLE III. Continuation of Table II.

r_s^-	N_e	N_μ	E_{VMC}	Var. of VMC	E_{DMC}	g(0)	$E_{c,v}$
2.5	50	10	−0.11678	0.34371	−0.12274	21.05	−0.00079217
2.5	50	20	−0.15498	0.84858	−0.17023	21.36	−0.0012726
2.5	50	30	−0.19848	1.0209	−0.20934	19.92	−0.0016751
2.5	50	40	−0.21420	1.5499	−0.23317	16.95	−0.0017716
2.5	50	50	−0.23403	1.6314	−0.24991	14.84	−0.0016966
2.5	20	40	−0.31422	0.46621	−0.32154	7.338	−0.0015353
2.5	20	60	−0.37877	0.84938	−0.38845	5.504	−0.0015073
2.5	10	40	−0.43661	0.26382	−0.44152	4.588	−0.0015627
2.5	10	50	−0.48113	0.27748	−0.48645	4.355	−0.0015056
2.5	8	80	−0.63925	0.27666	−0.64447	3.012	−0.0017843
3	50	10	−0.13118	0.29548	−0.13561	39.54	−0.00050355
3	50	20	−0.15695	0.8430	−0.17277	32.77	−0.00075110
3	50	30	−0.20074	0.94993	−0.21377	35.39	−0.0011199
3	50	40	−0.20904	2.0101	−0.22748	29.81	−0.0011406
3	50	50	−0.22925	1.1362	−0.24254	22.3	−0.0011754
3	20	40	−0.27854	0.45654	−0.28823	11.31	−0.00096176
3	20	60	−0.33447	0.37753	−0.33923	7.895	−0.00093066
3	10	40	−0.37560	0.20156	−0.380328	7.249	−0.00093910
3	10	50	−0.41247	0.20693	−0.417078	5.993	−0.00092946
3	8	80	−0.54136	0.19328	−0.54551	4.261	−0.00098069
4	50	10	−0.13389	0.21792	−0.141213	79.2	−0.00023542
4	50	20	−0.17292	0.40531	−0.186722	82.8	−0.00043639
4	50	30	−0.20137	0.77837	−0.214190	83.0	−0.00057497
4	50	40	−0.22669	1.8108	−0.249600	86.1	−0.00080102
4	50	50	−0.21379	2.8923	−0.253479	69.5	−0.00084602
4	20	40	−0.23935	0.43204	−0.247805	29.64	−0.00053030
4	20	60	−0.26798	0.29127	−0.274671	16.55	−0.00045265
4	10	40	−0.29654	0.23315	−0.301643	13.78	−0.00043827
4	10	50	−0.31192	0.26347	−0.325029	10.86	−0.00038674
4	8	80	−0.41570	0.23299	−0.419468	6.84	−0.00040340
3	50	10	−0.13211	0.31458	−0.138133	152	−0.00059900
5	50	20	−0.17467	0.35618	−0.183428	157	−0.00024381
5	50	30	−0.20189	0.61550	−0.213352	156	−0.00034042
5	50	40	−0.20374	1.5759	−0.227992	161	−0.00039366
5	50	50	−0.21729	1.6893	−0.242832	195	−0.00045757
5	20	40	−0.20284	0.33349	−0.219094	65.0	−0.00030663
5	20	60	−0.22351	0.48179	−0.233212	38.8	−0.00027496
5	10	40	−0.23978	0.23380	−0.248893	26.44	−0.00020729
5	10	50	−0.26583	0.17423	−0.273128	19.57	−0.00027533
5	8	80	−0.33802	0.16793	−0.342108	10.01	−0.00022212

the known $V^+(\mathbf{r})$ from the electronic part, thus no wave function basis for the muon is necessary. Another reason to use real space is that the boundary condition of the localized muon is easy to be set in real space. Otherwise, the muon would distribute at many local sites of the crystal with very low local density; this is not the physical image we expect.

In the electronic part of QE, a $3 \times 3 \times 3$ supercell was used for metals and diamond, while a $2 \times 2 \times 2$ supercell was used for CaF_2 and NaF, with the Perdew-Burke-Ernzerhof (PBE) [26] functional and optimized norm-conserving Vanderbilt (ONCV) [27] pseudopotentials. The cutoff of the wave function is not less than 120 Ry. A uniform Monkhorst-Pack [28] mesh grid was used for the k points. ($4 \times 4 \times 4$ for CaF_2, NaF and diamond, $6 \times 6 \times 6$ for metals. The magnetic moment per atom without muon is examined before calculation in metals.)

As for the FD method for the muon, it is iterated by [25]

$$\psi_{i,j,k}^{N+1} = \frac{\sum_{l,m,n} \psi_{lmn}^{N}}{6 + 2Mh^2(V_{ijk} - E^N)}, \tag{20}$$

$$E^N = \frac{\sum_{i,j,k} \left[\sum_{l,m,n} \psi_{lmn}^{N} - 6\psi_{ijk}^{N} + V_{ijk} \left| \psi_{ijk} \right|^2 \right]}{\sum_{ijk} \left| \psi_{ijk}^{N} \right|^2}, \tag{21}$$

$$\psi_{\mathrm{error}} = \sum_{ijk} \left| \psi_{ijk} \right|^2 \cdot \frac{|\mathrm{eq\_left} - \mathrm{eq\_right}|}{|\mathrm{eq\_right}|}, \tag{22}$$

where the indices i, j, k enumerate the real-space mesh; l, m, n run over the nearest neighbors of (i, j, k), six points in total. M is the mass of the muon, h is the pace of mesh, N is the iteration step number, V is the total potential of the muon, and E is the eigenenergy of the muon. In the iteration error

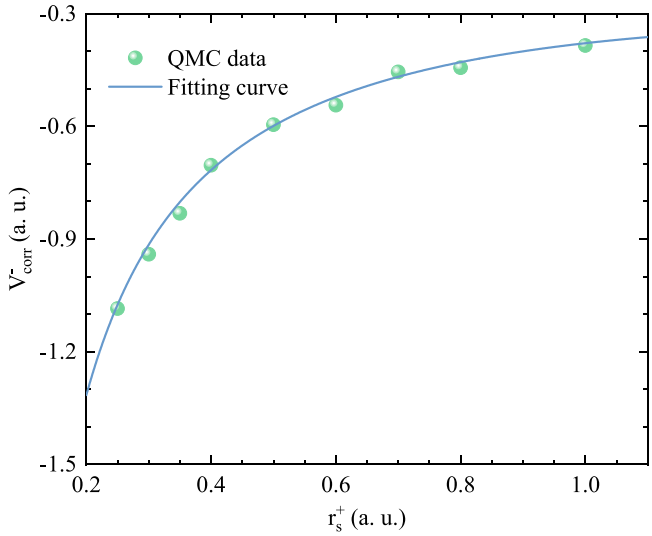

FIG. 4. Correlation potential of electrons calculated from 54 muons and 2 electrons. This corresponds to V_2 in Eq. (16).

estimation, eq_left and eq_right are the left side and right side of Eq. (2), at (i, j, k). The convergence threshold is 10^{-4} for ψ_{error} and 10^{-9} Ry for E^N–E^{N-1}. Note that this FD method requires an orthogonal lattice. If one has a nonorthogonal

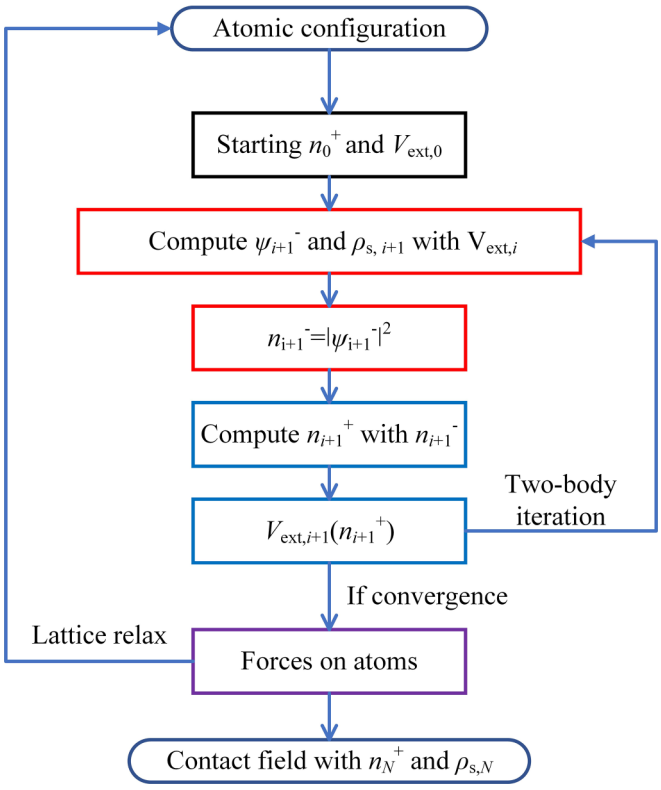

FIG. 5. TCDFT loop. + stands for muon, − stands for electrons. At present, the lattice optimization calculation using muon density (the arrow of lattice relax) is not implanted due to the calculation efficiency, the point-like muon optimization structure is simply applied in this work. Further study about the full relax calculation should be improved in the future.

TABLE IV. Hyperfine couplings in vacuum with different α.

α	0.5	0.8	1.0	1.2	1.5	2.0
A (MHz)	4429	4445	4455	4465	4472	4482

lattice, the localized muon space is interpolated to an orthogonal space to calculate the wave function of the muon, then after the FD calculation the wave function is interpolated back to the lattice basis.

Then the density of the muon and the electrons are replaced alternately until the calculated hyperfine couplings almost do not change. In this work, about five two-body cycles are applied for each material, thus the final error is under 0.005 Tesla or 10 MHz.

V. RESULTS AND DISCUSSION

As mentioned above, a semi-empirical parameter α is necessary due to the lack of high-density data. To find a good α, several values of α are used in a vacuum (use a fake hydrogen atom in a vacuum, as discussed, followed for the muonium case) and we find the hyperfine constant A is very close to the experiment if α is simply set to be 1 (considering that both the calculation and experiments have an error, we simply choose it to be a simple number within the error bar of the calculation instead of according to the experiments perfectly.) Some results are shown in Table IV. The convergent density of $\alpha = 1$ is shown in Fig. 6. The calculated A is 4455 MHz, while the point-like muon result is 4711 MHz and the experiment data are 4463 MHz. So we fix its value to be 1 in all calculations of this work. Note that the $g(0)$ of this work is not multiplied by $N/(N+1)$ [20], where N is the total number of particles in a system. If this correction is chosen, the α would be smaller, the final results would not change obviously due to the offset of $g(0)$ and the calculated contact spin density.

As an example of the muonium case, we calculate three simple nonmetallic materials with different crystal structures.

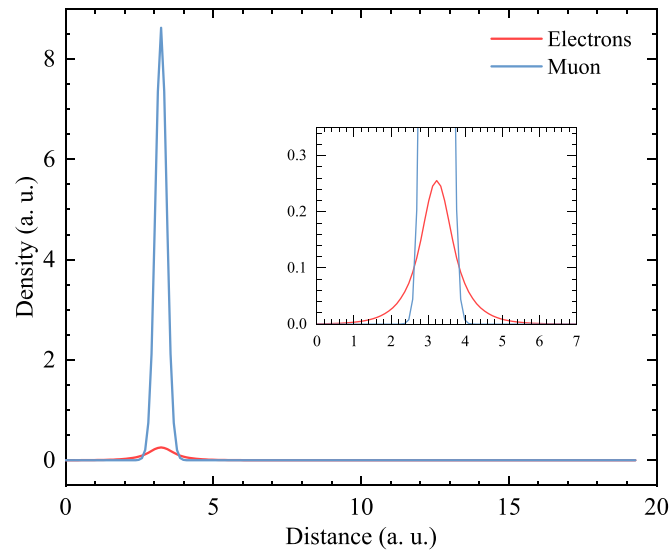

FIG. 6. Convergent density of vacuum for $\alpha = 1$.

TABLE V. Results of contact magnetic field (Tesla) or contact hyperfine coupling (MHz). Note that all calculated results in this work have an error bar of ∼0.005 Tesla or 10 MHz due to the TCDFT convergence fluctuation.

Material	Point-like muon[a]	Phonon-corrected[b]	This work	Experiment[c]
Fe-bcc	−1.25 T	−1.07 T	−1.076 T	−1.11 T
Co-hcp	−0.73 T	−0.68 T	−0.603 T	−0.58 T
Co-fcc	−0.79 T	−0.64 T	−0.614 T	−0.61 T
NaF	4389 MHz	4293 MHz	4513 MHz	4642 MHz
CaF_2	4610 MHz	4564 MHz	4469 MHz	4479 MHz
Diamond	4251 MHz	3597 MHz	4088 MHz	3711 MHz
Vacuum	4711 MHz		4455 MHz	4463 MHz

[a]References [2,5,29].
[b]References [2,7,29].
[c]References [30–35].

A hydrogen atom is defined at the muon site, but the pseudopotential of this hydrogen is reduced in the total potential. That means, in this case, Eq. (18) is changed to be

$$V_{\text{ext}}(\mathbf{r}') = \int \frac{n^+(\mathbf{r})\mathrm{d}^3\mathbf{r}}{|\mathbf{r}-\mathbf{r}'|} + V^-_{\text{corr}}(\mathbf{r}') - V_{ps,H}(\mathbf{r}'). \tag{23}$$

Since the plane-wave basis and the starting wave function of electrons in QE are expanded by the atoms' positions, a group of plane-wave expansion and a starting polarization around the muon site are defined by this method, thus the electronic orbits around muon are diagonalized as a hydrogen-like orbit with the center at the muon site. If this method is not chosen, the electronic plane-wave orbits are only expanded by the atoms of the host material, thus the electrons are treated as "superpositions of other atomic orbits with just an external potential around the muon sites." These two methods can give different convergent results because the wave-function basis and the starting density are completely different. Intuitively, the muonium state is close to the hydrogen-like state, thus the "fake hydrogen" method is applied. In fact, if this method is not applied, the polarization of the electrons around muon sites cannot be found by LSDA. This may be why point-like muon results in fluorides are not far from the experiments in the muonium case due to the similar orbit states.

The calculated contact hyperfine couplings above are in Table V. The convergent results of TCDFT show that the wave function of the muon is close to being a Gaussian although we did not fix its form. The local density of the muon is obviously larger than in phonon-corrected methods. Even though point-like muon or phonon methods are able to acquire good agreements with experiments, TCDFT is not worse than them with the semi-empirical parameter α.

In the case of μ^+ in metals, the contact field appears due to the magnetization of the host materials. However, different from the muonium case, the polarization of electrons is close to point-like results whether a hydrogen atom at the muon site is defined. If a hydrogen atom is defined, the contact field results are −1.261 T, −0.717 T, and −0.750 T for Fe-bcc, Co-hcp, and Co-fcc, respectively. These results are close to the point-like muon case. If a hydrogen atom is not defined, the contact field results become smaller and show wonderful

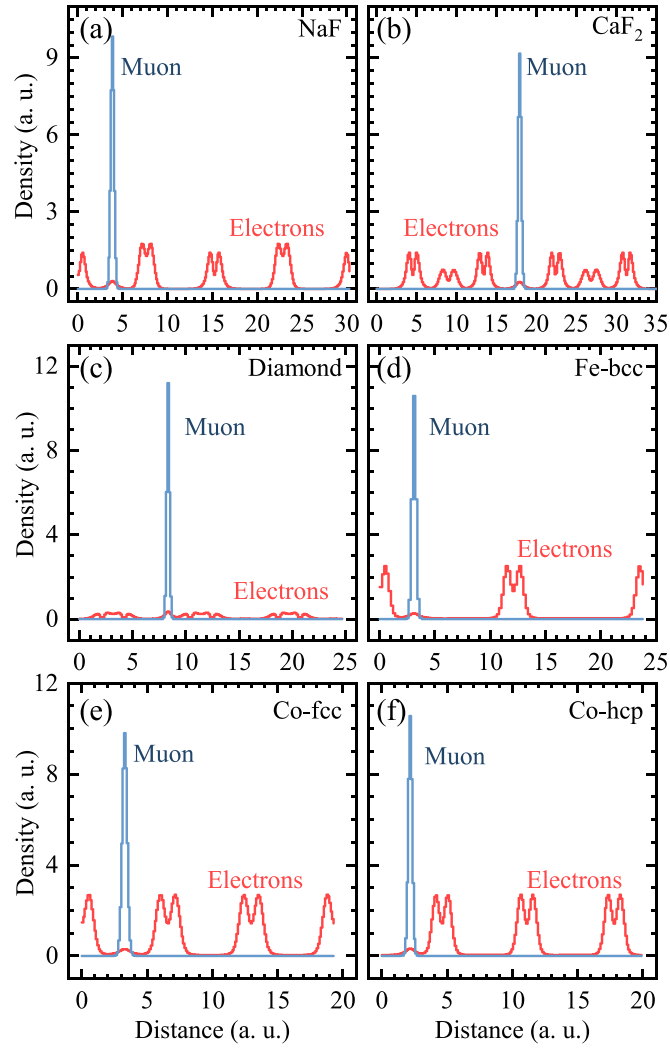

FIG. 7. Convergent density for (a) NaF, plotted from (0,0,0) to (2,2,2), muon site is $(\frac{1}{4},\frac{1}{4},\frac{1}{4})$. (b) CaF_2, from (0,0,0) to (2,2,2), muon site is (1,1,1). (c) Diamond, from (0,0,0) to (2,2,2), muon site is $(\frac{2}{3},\frac{2}{3},\frac{2}{3})$. (d) Fe-bcc, from (0,0,0) to (2,1,0), muon site is $(\frac{1}{2},\frac{1}{4},0)$. (e) Co-fcc, from $(0,\frac{1}{2},\frac{1}{2})$ to $(3,\frac{1}{2},\frac{1}{2})$, muon site is $(\frac{1}{2},\frac{1}{2},\frac{1}{2})$. (f) Co-hcp, from $(0,1,\frac{3}{4})$ to $(3,-2,\frac{3}{4})$, muon site is $(\frac{1}{3},\frac{2}{3},\frac{3}{4})$. Crystal structures with the muon can be found in Refs. [1,5,29].

agreements with the experiments (see Table V). As discussed above, while the muon is thought to be bare in this case, it would be better not to define such a fake hydrogen atom and the contact field results agree with that. This may be also why the point-like results are obviously bigger and not as good as it is in the muonium case. All convergent density results above are shown in Fig. 7.

Thus, TCDFT is tested in some basic systems and the results are surprisingly good, the errors compared with other works are shown in Fig. 8. There are still some possible ways to improve the accuracy.

(1) Use the wave function of the muon to optimize the lattice structure until getting fully convergent.

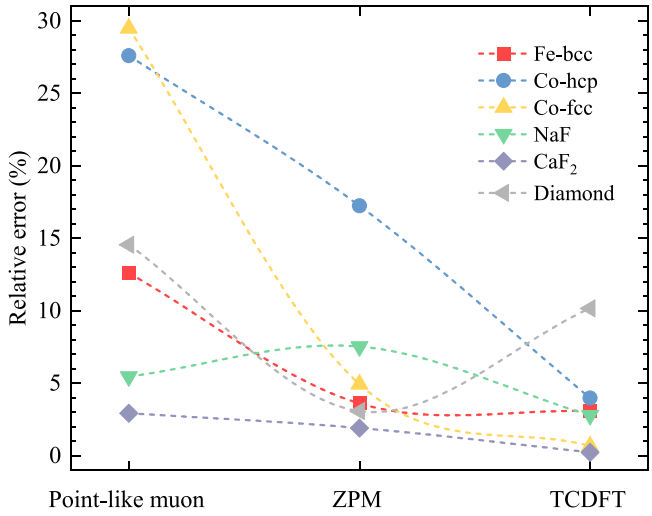

FIG. 8. Relative errors of different methods. Dashed curves are a guide to the eye.

(2) Further study about the two-body correlation functional. Develop an accurate $V_{\text{corr}}^{\pm}$ for all regions of n^{+} and n^{-}, especially for the high-R region. Or try to use some approximation beyond LDA (GGA, for example).

(3) Use some mixing method to iterate the two-body density instead of direct replacements.

Finally, we establish the calculation frame for muon-electron system within TCDFT and do some example calculations in basic systems. The calculation errors of this work mainly come from the formula of the two-body correlation energy and the PCF (as well as the exponential approximation of the correlation potential), this may be the most obvious weakness of TCDFT. However, on the one hand, such an approximation is already better than the point-like muon and phonon methods. On the other hand, the parametric form is adjustable, it would be possible to change its formula or include an empirical parameter to achieve the purpose of calculating correctly for a specific species of materials. Thus, TCDFT shows its good potential for further such calculations in studying the quantum effect of the particles like muon in materials.

ACKNOWLEDGMENTS

This work was financially supported by the National Key R&D Program of China (Grant No. 2019YFA0210000) and the National Natural Science Foundation of China (Grant No. 12005221). Computing resources were mainly provided by the STFC Scientifc Computing Department's SCARF cluster. The authors would like to thank N. D. Drummond from the Department of Physics, Lancaster University for valuable discussion.

[1] J. Möller, P. Bonfà, D. Ceresoli, F. Bernardini, S. Blundell, T. Lancaster, R. De Renzi, N. Marzari, I. Watanabe, S. Sulaiman *et al.*, Playing quantum hide-and-seek with the muon: Localizing muon stopping sites, Phys. Scr. **88**, 068510 (2013).

[2] J. S. Möller, D. Ceresoli, T. Lancaster, N. Marzari, and S. J. Blundell, Quantum states of muons in fluorides, Phys. Rev. B **87**, 121108(R) (2013).

[3] F. Bernardini, P. Bonfa, S. Massidda, and R. De Renzi, Ab initio strategy for muon site assignment in wide band gap fluorides, Phys. Rev. B **87**, 115148 (2013).

[4] P. Bonfà and R. De Renzi, Toward the computational prediction of muon sites and interaction parameters, J. Phys. Soc. Jpn. **85**, 091014 (2016).

[5] I. J. Onuorah, P. Bonfà, and R. De Renzi, Muon contact hyperfine field in metals: A dft calculation, Phys. Rev. B **97**, 174414 (2018).

[6] L. Liborio, S. Sturniolo, and D. Jochym, Computational prediction of muon stopping sites using ab initio random structure searching (airss), J. Chem. Phys. **148**, 134114 (2018).

[7] I. J. Onuorah, P. Bonfà, R. De Renzi, L. Monacelli, F. Mauri, M. Calandra, and I. Errea, Quantum effects in muon spin spectroscopy within the stochastic self-consistent harmonic approximation, Phys. Rev. Mater. **3**, 073804 (2019).

[8] J. M. Wilkinson and S. J. Blundell, Information and Decoherence in a Muon-Fluorine Coupled System, Phys. Rev. Lett. **125**, 087201 (2020).

[9] M. Gomilšek, F. Pratt, S. Cottrell, S. Clark, and T. Lancaster, Many-body quantum muon effects and quadrupolar coupling in solid nitrogen, arXiv:2202.05859.

[10] B. Monserrat, N. D. Drummond, and R. J. Needs, Anharmonic vibrational properties in periodic systems: Energy, electron-phonon coupling, and stress, Phys. Rev. B **87**, 144302 (2013).

[11] M. J. Puska and R. M. Nieminen, Theory of positrons in solids and on solid surfaces, Rev. Mod. Phys. **66**, 841 (1994).

[12] R. M. Nieminen, E. Boronski, and L. J. Lantto, Two-component density-functional theory: Application to positron states, Phys. Rev. B **32**, 1377(R) (1985).

[13] E. Boroński and R. M. Nieminen, Electron-positron density-functional theory, Phys. Rev. B **34**, 3820 (1986).

[14] J. Wiktor, G. Jomard, and M. Torrent, Two-component density functional theory within the projector augmented-wave approach: Accurate and self-consistent computations of positron lifetimes and momentum distributions, Phys. Rev. B **92**, 125113 (2015).

[15] P. E. Blöchl, Projector augmented-wave method, Phys. Rev. B **50**, 17953 (1994).

[16] D. M. Ceperley and B. J. Alder, Ground State of the Electron Gas by a Stochastic Method, Phys. Rev. Lett. **45**, 566 (1980).

[17] W. Foulkes, L. Mitas, R. Needs, and G. Rajagopal, Quantum monte carlo simulations of solids, Rev. Mod. Phys. **73**, 33 (2001).

[18] R. J. Needs, M. D. Towler, N. D. Drummond, P. López Ríos, and J. R. Trail, Variational and diffusion quantum monte carlo calculations with the casino code, J. Chem. Phys. **152**, 154106 (2020).

[19] M. Goli and S. Shahbazian, Two-component density functional theory for muonic molecules: Inclusion of the electron–positive

muon correlation functional, J. Chem. Phys. **156**, 044104 (2022).
[20] N. D. Drummond, P. Lopez Ríos, R. J. Needs, and C. J. Pickard, Quantum Monte Carlo Study of a Positron in an Electron Gas, Phys. Rev. Lett. **107**, 207402 (2011).
[21] Y. Kwon, D. M. Ceperley, and R. M. Martin, Effects of backflow correlation in the three-dimensional electron gas: Quantum monte carlo study, Phys. Rev. B **58**, 6800 (1998).
[22] P. López Ríos, A. Ma, N. D. Drummond, M. D. Towler, and R. J. Needs, Inhomogeneous backflow transformations in quantum monte carlo calculations, Phys. Rev. E **74**, 066701 (2006).
[23] C. J. Umrigar, J. Toulouse, C. Filippi, S. Sorella, and R. G. Hennig, Alleviation of the Fermion-Sign Problem by Optimization of Many-Body Wave Functions, Phys. Rev. Lett. **98**, 110201 (2007).
[24] P. Giannozzi, S. Baroni, N. Bonini, M. Calandra, R. Car, C. Cavazzoni, D. Ceresoli, G. L. Chiarotti, M. Cococcioni, I. Dabo *et al.*, Quantum espresso: A modular and open-source software project for quantum simulations of materials, J. Phys.: Condens. Matter **21**, 395502 (2009).
[25] M. J. Puska and R. M. Nieminen, Theory of hydrogen and helium impurities in metals, Phys. Rev. B **29**, 5382 (1984).
[26] J. P. Perdew, K. Burke, and M. Ernzerhof, Generalized Gradient Approximation Made Simple, Phys. Rev. Lett. **77**, 3865 (1996).
[27] D. R. Hamann, Optimized norm-conserving vanderbilt pseudopotentials, Phys. Rev. B **88**, 085117 (2013).
[28] H. J. Monkhorst and J. D. Pack, Special points for brillouin-zone integrations, Phys. Rev. B **13**, 5188 (1976).
[29] R. H. Luchsinger, Y. Zhou, and P. F. Meier, Gradient corrections in first-principles calculations of hyperfine parameters in semiconductors, Phys. Rev. B **55**, 6927 (1997).
[30] H. Graf, W. Kündig, B. Patterson, W. Reichart, P. Roggwiller, M. Camani, F. Gygax, W. Rüegg, A. Schenck, H. Schilling *et al.*, Local Magnetic Field at a Positive Muon in Ferromagnetic Cobalt, Phys. Rev. Lett. **37**, 1644 (1976).
[31] N. Nishida, R. Hayano, K. Nagamine, T. Yamazaki, J. Brewer, D. Garner, D. Fleming, T. Takeuchi, and Y. Ishikawa, Hyperfine field and diffusion of $\mu+$ in fe single crystals, Solid State Commun. **22**, 235 (1977).
[32] B. Lindgren and D. E. Ellis, Hyperfine fields and electronic structure of hydrogen impurities in transition metals, Phys. Rev. B **26**, 636 (1982).
[33] R. F. Kiefl, E. Holzschuh, H. Keller, W. Kündig, P. F. Meier, B. D. Patterson, J. W. Schneider, K. W. Blazey, S. L. Rudaz, and A. B. Denison, Decoupling of Muonium in High Transverse Magnetic Fields, Phys. Rev. Lett. **53**, 90 (1984).
[34] H. Baumeler, R. Kiefl, H. Keller, W. Kündig, W. Odermatt, B. Patterson, J. Schneider, T. Estle, S. Rudaz, D. Spencer *et al.*, Muonium centers in the alkali halides, Hyperfine Interact. **32**, 659 (1986).
[35] E. Holzschuh, W. Kündig, P. F. Meier, B. D. Patterson, J. P. F. Sellschop, M. C. Stemmet, and H. Appel, Muonium in diamond, Phys. Rev. A **25**, 1272 (1982).